Acoustic emission monitoring of hydraulic fracturing laboratory experiment with supercritical and liquid CO_2

Tsuyoshi Ishida,[1] Kazuhei Aoyagi,[1] Tomoya Niwa,[1] Youqing Chen,[2] Sumihiko Murata,[1] Qu Chen,[3] and Yoshiki Nakayama[3]

Received 21 June 2012; revised 21 July 2012; accepted 24 July 2012; published 29 August 2012.

[1] Carbon dioxide (CO_2) is often used for enhanced oil recovery in depleted petroleum reservoirs, and its behavior in rock is also of interest in CO_2 capture and storage projects. CO_2 usually becomes supercritical (SC-CO_2) at depths greater than 1,000 m, while it is liquid (L-CO_2) at low temperatures. The viscosity of L-CO_2 is one order lower than that of normal liquid water, and that of SC-CO_2 is much lower still. To clarify fracture behavior induced with injection of the low viscosity fluids, we conducted hydraulic fracturing experiments using 17 cm cubic granite blocks. The AE sources with the SC- and L-CO_2 injections tend to distribute in a larger area than those with water injection, and furthermore, SC-CO_2 tended to generate cracks extending more three dimensionally rather than along a flat plane than L-CO_2. It was also found that the breakdown pressures for SC- and L-CO2 injections are expected to be considerably lower than for water. **Citation:** Ishida, T., K. Aoyagi, T. Niwa, Y. Chen, S. Murata, Q. Chen, and Y. Nakayama (2012), Acoustic emission monitoring of hydraulic fracturing laboratory experiment with supercritical and liquid CO_2, *Geophys. Res. Lett.*, *39*, L16309, doi:10.1029/2012GL052788.

1. Introduction

[2] Carbon dioxide (CO_2) is injected into the underground rock for a variety of purposes. It is often used for miscible flooding to enhance oil recovery in depleted petroleum reservoirs, and the use of CO_2 as a fracturing fluid for well stimulation has been considered because it eliminates formation damage and residual fracturing fluid [*Sinal and Lancaster*, 1987; *Liao et al.*, 2009]. Using CO_2 for fracturing and as a circulating fluid has also been proposed in hot dry rock geothermal energy extraction, because it reduces the circulating pumping power requirements and eliminates scaling in the surface piping due to the inability of CO_2 to dissolve mineral species [*Brown*, 2000]. Recently, the possibility of combining CO_2 sequestration with the injection of CO_2 to enhance recovery from shale gas reservoirs has been examined [*Kalantari-Dahaghi*, 2010]. For all of these purposes it is necessary to understand the behavior of CO_2 in rock. It is also important to know how injected CO_2 will infiltrate into the surrounding rock mass in CO_2 capture and storage projects [*Xue et al.*, 2006; *Nooner et al.*, 2007].

[3] In these projects, CO_2 is usually injected into rocks at a depth of more than 1,000 m. The temperature and pressure at that depth usually makes CO_2 a supercritical state, while the lower temperatures in special geological conditions create a liquid state. The viscosity of liquid CO_2 is one order lower than that of normal liquid water, while that of the supercritical state is much lower still. To clarify fracture behavior induced with injection of the low viscosity fluid, we conducted hydraulic fracturing experiments using supercritical CO_2 (SC-CO_2) and liquid CO_2 (L-CO_2). We discussed the breakdown pressure and distribution of located acoustic emission (AE) sources of the experiments in comparison with those with water and viscous oil injections in the previous similar experiments [*Ishida et al.*, 2004].

2. Experimental Method

2.1. Specimens and Confining Pressure

[4] Four cubic (17 cm × 17 cm × 17 cm) samples of Kurokami-jima granite were used as specimens. Two of the four, the specimens G1009 and G1010, were subjected to SC-CO_2 injection, while the other two, the specimens G1011 and G1012, were subjected to L-CO_2 injection. The samples had a 2 cm diameter central hole, and the inherent rift plane of the granite specimen was oriented so as to correspond to the YZ-plane in the Cartesian coordinate system, as shown in Figure 1a. P-wave velocities measured along the Y- and Z-directions were around 5.0 km/s, while that along the X-direction normal to the rift plane was around 4.3 km/s. To monitor AE events induced with the injection, sixteen cylindrical PZT elements in total were glued on the six surfaces of the specimen. To apply confining pressures, the specimen, together with the PZT elements on its surfaces, was encapsulated in plaster.

[5] The specimen was placed in a cylindrical pressure cell. Four bow-shaped spacer blocks were inserted between the specimen and the inner wall of the pressure cell, and a flat jack was placed between the specimen and each spacer block to apply pressure in the X- and Y-directions. In the Z-direction, flat jacks were placed between the specimen and loading plates supported by the end caps on the top and bottom of the pressure cell. In all experiments, confining pressures of 1 MPa were applied in the X-, Y- and Z- directions to provide the hydrostatic stress condition. Figure 1b shows the packer used to inject CO_2 which was inserted into the center hole of the samples. The packer had a 60 mm pressurizing section sealed with two O-rings at each end. The pressurizing section was centered along the hole.

[1]Department of Civil and Earth Resource Engineering, Graduate School of Engineering, Kyoto University, Kyoto, Japan.
[2]Department of Energy Science and Technology, Graduate School of Energy Science, Kyoto University, Kyoto, Japan.
[3]3D Geoscience, Inc., Tokyo, Japan.

Corresponding author: T. Ishida, Department of Civil and Earth Resources Engineering, Graduate School of Engineering, Kyoto University, Kyoto, 615-8540, Japan. (ishida.tsuyoshi.2a@kyoto-u.ac.jp)

0094-8276/12/2012GL052788

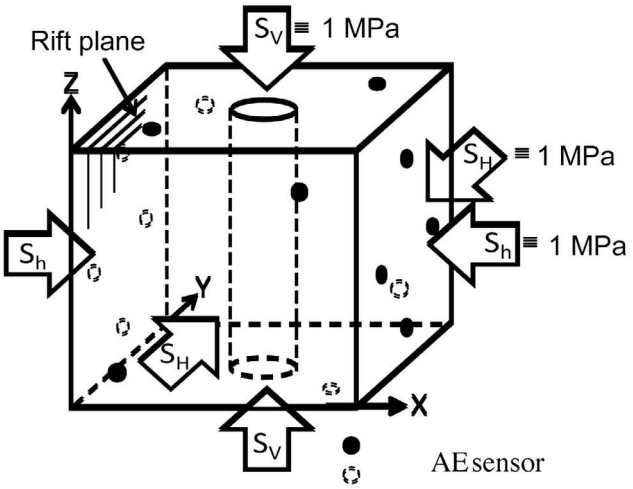

(a)

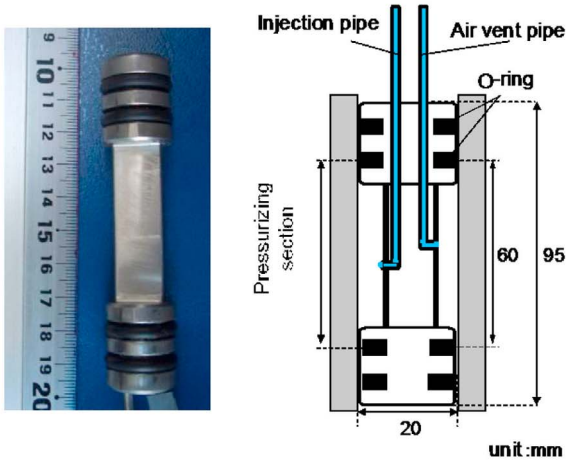

(b)

Figure 1. Specimen and straddle packer used to inject CO_2. (a) Specimen, loading condition and positions of AE sensors. (b) Photo and illustration of a sectional view of the packer.

2.2. CO_2 Injection Method

[6] To control the experimental conditions, the injection system shown in Figure 2 was made especially for these experiments. The CO_2 was fed from a bomb to a cylinder of the syringe pump, which has a capacity of 266 mL. To fill the cylinder as full as possible, the CO_2 was cooled and kept in liquid form by circulating coolant in a cooling unit located above the cylinder. L-CO_2 was discharged from the cylinder of the syringe pump at a constant flow rate of 30 mL/min, to be injected into the packer placed in a hole in the center of the specimen. The injection was stopped just after hydraulic fracturing was induced, which was indicated by a sudden pressure drop. CO_2 becomes supercritical when the temperature is higher than 31.1°C and the pressure is greater than 7.38 MPa, while it is liquid at lower temperatures. For SC-CO_2 induced fracturing, the L-CO_2 discharged from the syringe pump was passed through a heater unit and the temperature was maintained at 55°C by bandaging electric resistance heating ribbon along the pipe connecting the heater unit to the packer as shown in Figure 2. In addition, the cell in which the specimen was contained was filled with hot water at a temperature of around 45°C to prevent the injected CO_2 from cooling. Although the specimen was soaked in hot water for around one hour, we believed that water does not infiltrate into around the injection hole due to its low permeability and the hydraulic fracturing was induced in dry condition from our experience on previous similar experiments. Thus, for the L-CO_2 injection, L-CO_2 was fed to the packer without heating and the cell was kept at room temperature without filling water.

2.3. Methods to Monitor AE, Pressure and Temperature

[7] The PZT elements glued onto the specimen were cylindrical, 3 mm in diameter and 4 mm in length, and had a resonance frequency of 300 kHz. They were covered with aluminum sheet to avoid electromagnetically induced noise. They were also covered with heat shrinkable tubes and silicon rubber to provide a waterproof barrier for the plaster encapsulation. The detected AE signals were amplified by 66 to 84 dB in total (36 dB in a pre-amplifier and 30 to 48 dB in a signal conditioner), and recorded on a hard disk through an A/D converter. For each event, the record length and sampling time of the A/D converter were selected to be 2048 words and 0.1 μs, respectively. The dead time was set to be 1 ms after recording an event, to prevent the hard disk from recording too much noise due to "ringing," which is the vibration following a large AE event. The recording of an AE event was triggered when one of the signals from 16 AE sensors exceeded 0.3 V. In addition, the number of AE events per second was counted for each AE sensor when the signal exceeded 0.3 V.

[8] Every 0.1 s, the injected CO_2 pressure was measured through transducers set at the top of the packer, and the flat jack pressures in the three directions, X, Y and Z, were measured through transducers set on the connecting pipes of opposing pairs of flat jacks. Temperature changes were measured with a thermocouple glued on the injection pipe just above the packer in the hole. Thermocouples were also

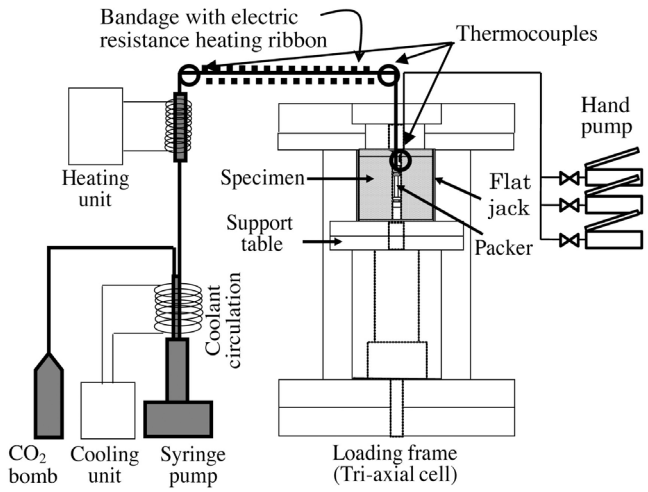

Figure 2. Injection system for SC-CO_2 and L-CO_2.

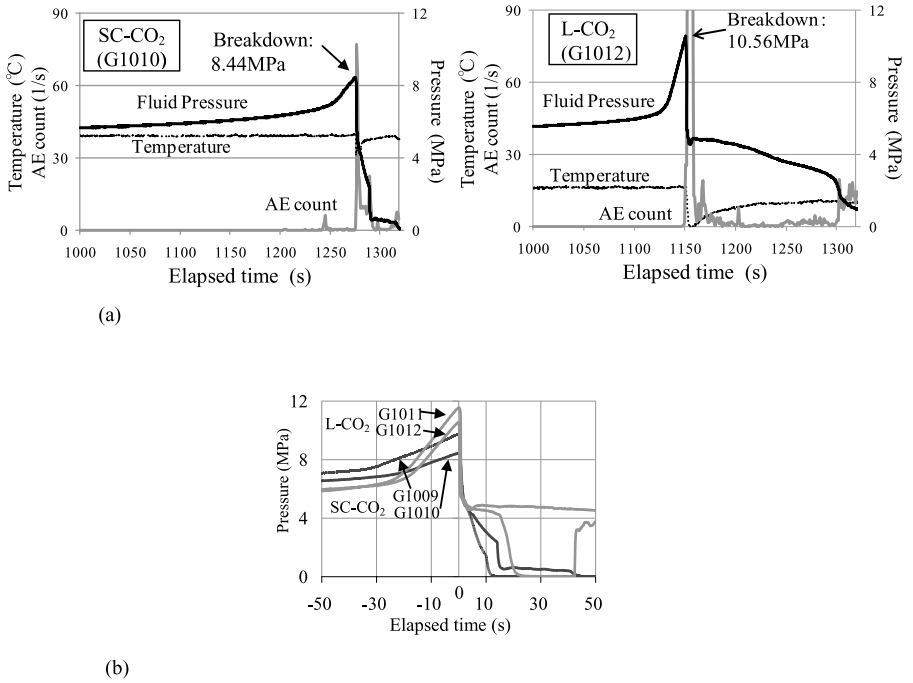

Figure 3. Change of injected fluid pressure, AE count rate and temperature. (a) Fluid pressure, AE count rate and temperature in typical examples of SC-C2 and L-CO2 injection. (b) Fluid pressure for 50 s just before and after the breakdown in all the experiments.

placed at the both ends of the section of a pipe covered with electric resistance heating ribbon, as shown in Figure 2.

3. Results and Discussion

3.1. Change of Fluid Pressure, Temperature and AE Count Rate

[9] Figure 3a shows changes of the injected fluid pressure, the AE count rate and the temperature when SC-CO_2 and L-CO_2 were injected into the specimens, G1010 and G1012, respectively. In the left plot, the temperature measured with a thermocouple glued onto the injection pipe just above the packer was 40.2°C, which indicates that the fracturing was induced by SC-CO_2. On the other hand, in the right plot, the temperature was 16.1°C, indicating that the fracturing was induced by L-CO_2. In both cases, the temperature decreased along with the breakdown pressure. This is most likely due to adiabatic expansion of CO_2 by leakage through the cracks created by the fracturing. The AE occurrence rose sharply just after the fracturing and events continued to occur for several seconds.

[10] Figure 3b shows change of the injected fluid pressure for 50 s just before and after the breakdown in all the experiments, including the records shown in Figure 3a. The breakdown pressures of 8.44 and 9.74 MPa recorded for SC-CO_2 are lower than those of 10.56 and 11.56 MPa for L-CO_2. A possible explanation is that a slick fluid, like SC-CO_2, having lower viscosity infiltrates into defects in the matrix around the hole more easily than L-CO_2. Although the injected flow rate was constant at 30 mL/min throughout the experiment for all cases, the pressure increases in L-CO_2 just before the breakdown are much steeper than those in SC-CO_2. To confirm this difference, we injected CO_2 into a steel pipe that is completely impermeable and has the same diameter as the hole. The flow rate and temperatures were set to be the same as in the experiment: the flow rate was 30 mL/min and the temperatures for SC-CO_2 and L-CO_2 were around 40 and 16°C respectively. The pressure changes showed the same sort of difference between SC-CO_2 and L-CO_2 as the cases shown in Figure 3b. Therefore, it can be concluded that the difference in the pressure changes is not caused by a difference in leak-off rate due to the difference in viscosity between SC-CO_2 and L-CO_2. The difference is most likely due to the difference in compressibility of the fluid, because SC-CO_2 is much more easily compressed than L-CO_2. This inference is also supported by the fact that the difference in the pressure change becomes noticeable after the pressure reached around 7.38 MPa where the CO_2 becomes supercritical at the temperature of the SC-CO_2 experiments. The steep increase in the pressure may help the breakdown pressures for L-CO_2 to become larger than those for SC-CO_2.

3.2. Induced Visible Cracks and Located AE Sources

[11] After the experiments, we closely observed the induced cracks on the specimen surfaces with the naked eye. Figures 4a and 4b show the visible cracks sketched on the unfolded planes of the specimens. The figure shows that the cracks were induced along the inherent rift plane for both SC-CO_2 (G1010) and L-CO_2 (G1012) injection. This also occurred in the other two specimens, G1009 and G1011, not shown in the figure. Figures 4c and 4d show the distribution of 95 and 78 AE sources for SC-CO_2 (G1010) and L-CO_2 (G1012), with an accuracy expected to fall within a few mm satisfying certain conditions [*Ishida and Sasaki*, 2011].

[12] The fractal dimensions of the distributions of the located sources were obtained by the correlation function method, following *Hirata et al.* [1987] and *Grassberger*

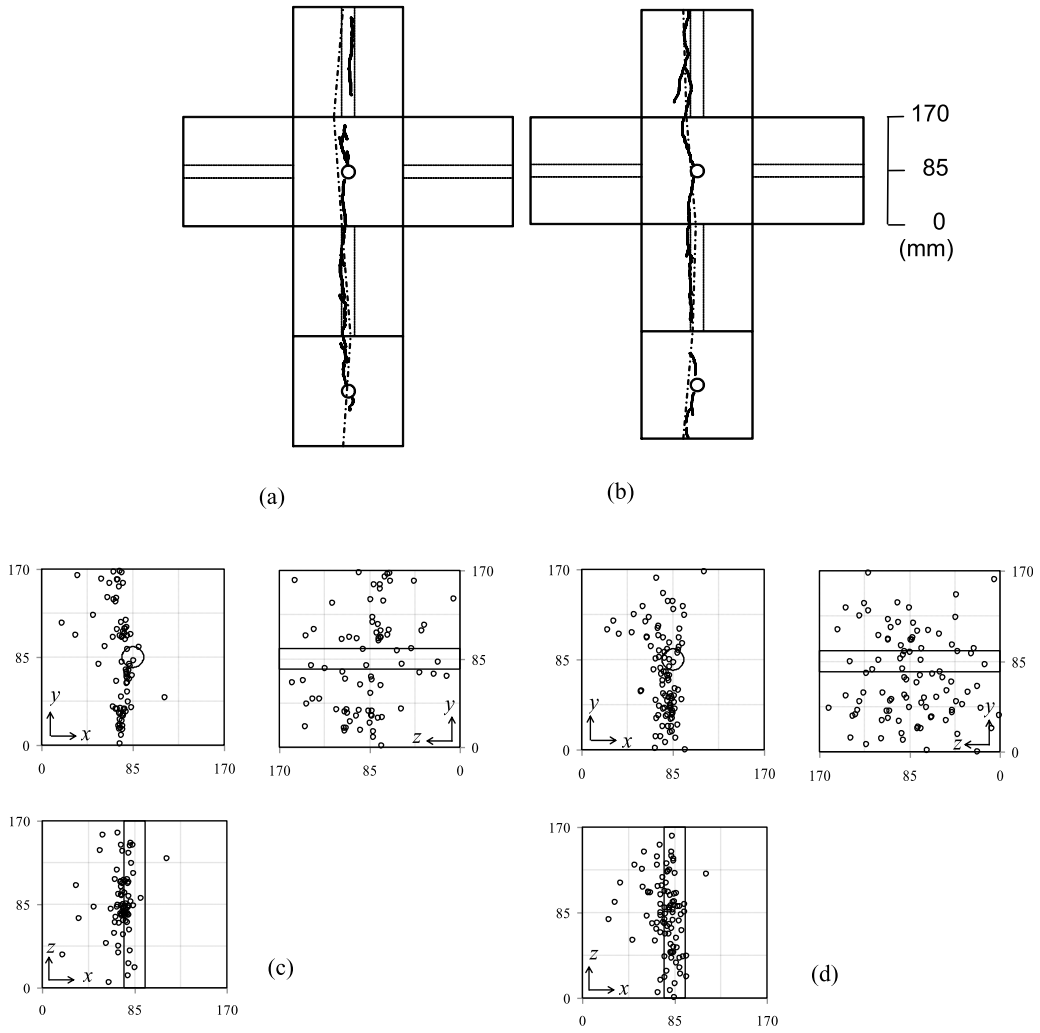

Figure 4. Cracks and AE source distributions for typical examples of SC-CO2 and L-CO2 injection. Cracks (bold lines) observed on the specimen surfaces and intersection lines (thin chain lines) of the most likely flat plane estimated from the source distribution: (a) SC-CO_2 (G1010) and (b) L-CO_2 (G1012). Projections of AE sources onto the *xy*-, *yz*- and *zx*-planes: (c) SC-CO_2 (G1010; FD = 2.20, L_{av} = 8.82 mm) and (d) L-CO_2 (G1012; FD = 1.64, L_{av} = 7.80 mm).

[1983]. Theoretically, the fractal dimension for infinite numbers of points distributed on a line, on a flat plane and three dimensionally should be one, two and three, respectively. Since a number of points distributed is limited, the fractal dimensions obtained with the method tend to be a little bit lower than the respective dimensions. However, the dimension still can measures fracture behavior, and in the case, the larger fractal dimension indicates that AE sources distributes the more three dimensionally rather than along a flat plane, suggesting the induced fracture extending the more three dimensionally. The fractal dimensions, *FD*, for SC-CO_2 fracturing were 2.20 in specimen G1010, while those for L-CO_2 were 1.64 in G1012. The fractal dimensions obtained in the other two experiments showed the same tendency (see Table 1).

[13] The most likely flat plane for the distribution of the AE sources was also estimated for each experiment, by minimizing the sum of squares of distances from a located source to the flat plane. The average distance from a source to the estimated flat plane, L_{av}, was 8.82 mm in the specimen G1010 (SC-CO_2), while that for G1012 (L-CO_2) was 7.80 mm. The average distances in the specimens G1009 (SC-CO_2) and G1011 (L-CO_2) showed the same pattern, being 24.2 mm and 7.80 mm, respectively. The large value of L_{av} in G1009 is due to a three dimensional AE source distribution particularly in a lower part of the specimen (not shown here). The most likely flat plane cuts across the four out of the six surface planes of the specimen. The intersection lines are also shown in Figures 4a and 4b. The intersection lines for L-CO_2 (Figure 4b) almost coincide with the visible cracks on the surfaces, while those for SC-CO_2 (Figure 4a)

Table 1. Number of Located AE Sources, the Fractal Dimension, *FD*, and the Average Distance to the Most Likely Flat Plane, L_{av}, Which Were Obtained for Each Experiment

Injectant	Specimen Number	Located AE Sources	*FD*	L_{av} (mm)
SC-CO_2	G1009	79	2.64	24.2
	G1010	95	2.20	8.82
L-CO_2	G1011	103	1.62	5.30
	G1012	78	1.64	7.80

do not show such a close correspondence. The wide variance of the source distribution for SC-CO_2 probably causes the larger gap between the intersection lines and the visible cracks. Although the observed difference in the distance *L*av, 1.02 mm, between SC-CO_2 (G1010) and L-CO_2 (G1012) is not large, it is consistent with the differences in the fractal dimensions and in the gaps between the visible cracks and the intersection lines. Thus, it seems to be significant and meaningful, suggesting the fracture induced with SC-CO_2 extends three dimensionally than that with L-CO_2, for example, wavelike with more secondary braches rather than along a flat plane.

3.3. Feature of Fracture Behavior in Comparison With Water Injection

[14] *Ishida et al.* [2004] conducted hydraulic fracturing experiments on the same kind of cubic Kurokami-jima granite using normal water and viscous oil, with viscosities of 1 and 80 mPa·s, respectively. The results indicate that viscous oil tends to generate thick and planar cracks with few branches, while water tends to generate thin and wavelike cracks with many secondary branches. The viscosities of SC-CO_2 and L-CO_2 at the fracturing are 0.025 and 0.088 mPa·s respectively. These values were calculated using the equation of state for CO_2 of T. Ohmori (http://hp.vector.co.jp/authors/VA030090/) based on the theory by *Fenghour et al.* [1998]. For the calculation, a temperature and pressure of 40.2°C and 8.44 MPa were used for SC-CO_2, while 16.1°C and 10.56 MPa were used for L-CO_2. Considering the difference of viscosities, it seems to be consistent that the fractal dimension and the average distance for located AE sources associated with SC-CO_2 injection are larger than those for L-CO_2. Furthermore, when we compare the source distributions with the SC- and L-CO_2 injections to those with water and oil injections in *Ishida et al.* [2004, Figures 6 and 7], we can easily find the distributions with SC- and L-CO_2 extend in a larger area than those with water and oil on projections of respective planes. On the other hand, *Warpinski et al.* [2005] produced hydraulic fracturing using gel and slick water in a shale gas reservoir, and compared the microseismic maps associated with the two fracturings. The map associated with slick water fracturing outlines a much larger area than that achieved with the gel fracturing. Our results including those in *Ishida et al.* [2004] are consistent with the field experience, from the viewpoint of the difference in the fracturing fluid viscosity.

[15] In the experiments by *Ishida et al.* [2004], the magnitude of the breakdown pressure for the viscous oil was 16.5 and that of water was 17.9 MPa, which was inconsistent with the fact that viscosity of the oil is 80 times larger than that of water. In this case, variation in the strengths of the specimens might cover the difference. Since the condition of confining pressures and flow rates are different between the experiments in this paper and those in *Ishida et al.* [2004], let's compare tensile strengths at the breakdown with subtracting the compressive stress induced at the fracturing point along the hole wall by the confining pressures using *Kirsch*'s [1898] solution, without considering pore pressure. The tensile strength in the SC- and L-CO_2 injections were 6.44 and 8.56 MPa, subtracting 2 MPa induced by the confining pressures that $S_H = 1$ and $S_h = 1$ from the breakdown pressure 8.44 MPa and 10.56 MPa, as shown in Figures 3a and 3b. On the other hand, the tensile strength in the water and oil injections in *Ishida et al.* [2004] were 14.9 and around 13.5 MPa, subtracting 3 MPa by $S_H = 6$ and $S_h = 3$ from the breakdown pressure 17.9 for water and 16.5 MPa for the viscous oil. Thus, the tensile strengths for the SC- and L-CO_2 injections are quite lower than those for the water and oil injections. Furthermore, the order of the tensile strengths almost follows the order of the injectant viscosities, with a slight reversal between water and the viscous oil. The results are consistent with the facts elucidated in experimentally by *Schmitt and Zoback* [1993] and theoretically by *Bunger et al.* [2010]. On the other hands, the difference in flow rates between 30 mL/min for the SC- and L-CO_2 injections and 10 mL/min for water and the oil injections does not seem to affect the results, because the larger flow rate should make the larger breakdown pressure [*Schmitt and Zoback*,1993; *Garagash and Detournay*, 1997]. Thus, under the same condition of in situ rock stress and flow rate, the breakdown pressure with CO_2 injection is expected to be considerably lower than with usual water injection due to its lower viscosity.

4. Conclusions

[16] Using SC- and L-CO_2 as the fracturing fluid, we conducted hydraulic fracturing experiments in cubic granite blocks. The results can be summarized as follows.

[17] (1) The fractal dimensions of the located AE source distributions with the SC-CO_2 injection were larger than those for L-CO_2 injection. Furthermore, the average distances from a source to the most likely flat plane estimated for the AE source distribution were also larger for SC-CO_2 than those for L-CO_2. These differences suggest that, due to its lower viscosity, SC-CO_2 tends to generate cracks extending more three dimensionally rather than along a flat plane than L-CO_2. (2) The AE source distributions were compared with those with water and viscous oil injections in the previous similar experiments. The AE sources with the SC- and L-CO_2 injections distributed in larger area more three dimensionally than those with water injection. The same difference was also observed in microseismic maps with hydraulic fracturing using gel and slick water in a shale gas reservoir, and our results is consistent with the filed experiences.

[18] (3) A tendency for the breakdown pressures to be lower for SC- than for L-CO_2 was observed. Comparison with water and the viscous oil injections elucidated that the breakdown pressures with SC- and L-CO_2 injections are expected to be considerably lower than with water injection due to their lower viscosities under the same in situ rock stress and flow rate.

[19] **Acknowledgments.** We would like to thank Ayaka Yamakawa and Yuya Nagaya, postgraduate students of Kyoto University, for their help and valuable discussions. This work was supported by JSPS (Japan Society for the Promotion of Science) Grant-in-Aid for Scientific Research (B), Grant Number 21360446.

[20] The Editor thanks one anonymous reviewer for assistance in evaluating this paper.

References

Brown, D. W. (2000), A hot dry rock geothermal energy concept utilizing supercritical CO_2 instead of water, paper presented at 25th Workshop on Geothermal Reservoir Engineering, Stanford Univ., Stanford, Calif.

Bunger, A. P., A. Lakirouhani, and E. Detournay (2010), Modelling the effect of injection system compressibility and viscous fluid flow on hydraulic fracture breakdown pressure, paper presented at 5th International Symposium on In-Situ Rock Stress, Int. Soc. for Rock Mech., Beijing.

Fenghour, A., W. A. Wakeham, and V. Vesovic (1998), The viscosity of carbon dioxide, *J. Phys. Chem. Ref. Data*, *27*(1), 31–44, doi:10.1063/1.556013.

Garagash, D., and E. Detournay (1997), An analysis of the influence of the pressurization rate on the borehole breakdown pressure, *Int. J. Solids Struct.*, *34*(24), 3099–3118, doi:10.1016/S0020-7683(96)00174-6.

Grassberger, P. (1983), Generalized dimensions of strange attractors, *Phys. Lett.*, *97A*(6), 227–230.

Hirata, T., T. Satoh, and K. Ito (1987), Fractal structure of spatial distribution of microfracturing in rock, *Geophys. J. R. Astron. Soc.*, *90*, 369–374, doi:10.1111/j.1365-246X.1987.tb00732.x.

Ishida, T., and S. Sasaki (2011), Numerical simulation to examine accuracy of AE source location and its applications to *in-situ* rock monitoring, *J. Acoust. Emission*, *29*, 260–272.

Ishida, T., Q. Chen, Y. Mizuta, and J.-C. Roegiers (2004), Influence of fluid viscosity on the hydraulic fracturing mechanism, *J. Energy Resour. Technol.*, *126*, 190–200, doi:10.1115/1.1791651.

Kalantari-Dahaghi, A. (2010), Numerical simulation and modeling of enhanced gas recovery and CO_2 sequestration in shale gas reservoirs: A feasibility study, paper presented at International Conference on CO_2 Capture, Storage, and Utilization, Soc. of Pet. Eng., New Orleans, La.

Kirsch, C. (1898), Die Theorie der Elastizität und die Bedürfnisse der Festigkeitslehre [in German], *Z. Ver. Dtsch. Ing.*, *42*, 797–807.

Liao, S., F. Brunner, and L. Mattar (2009), Impact of ignoring CO_2 injection volumes on post-frac PTA, paper presented at Canadian International Petroleum Conference, Pet. Soc. of Can., Calgary, Alberta, Canada.

Nooner, S. L., O. Eiken, C. Hermanrud, G. S. Sasagawa, T. Stenvold, and M. A. Zumberge (2007), Constraints on the in situ density of CO_2 within the Utsira formation from time-lapse seafloor gravity measurements, *Int. J. Greenhouse Gas Control*, *1*, 198–214, doi:10.1016/S1750-5836(07)00018-7.

Schmitt, D. R., and M. D. Zoback (1993), Infiltration effects in the tensile rupture of thin walled cylinders of glass and granite: Implications for the hydraulic fracturing breakdown equation, *Int. J. Rock Mech. Min. Sci. Geomech. Abstr.*, *30*, 289–303, doi:10.1016/0148-9062(93)92731-5.

Sinal, M. L., and G. Lancaster (1987), Liquid CO_2 fracturing: Advantages and limitations, *J. Can. Pet. Technol.*, *26*(5), 26–30.

Warpinski, N. R., R. C. Kramm, J. R. Heinze, and C. K. Waltman (2005), Comparison of single- and dual-array microseismic mapping techniques in the Barnett shale, paper presented at 2005 Annual Technical Conference and Exhibition, Soc. of Pet. Eng., Dallas, Tex.

Xue, Z., D. Tanase, and J. Watanabe (2006), Estimation of CO_2 saturation from time-lapse CO_2 well logging in an onshore aquifer, Nagaoka, Japan, *Explor. Geophys.*, *37*, 19–29, doi:10.1071/EG06019.